9-2018

Conformational analysis of a TADDOL-based phosphoramidite P,N ligand in a palladium(II) η3-π-allyl complex

Tülay A. Ateşin

Abdurrahman Atesin

Oscar Rodriguez

Diego Rivera

Lohany Y. Garcia

Version of Record: https://www.sciencedirect.com/science/article/pii/S2210271X18302731
Manuscript_103f28518caa59ea17d31c7235b6a889

Conformational analysis of a TADDOL-based phosphoramidite *P*,*N* ligand in a palladium(II) η^3-π-allyl complex

Tülay A. Ateşin,* Abdurrahman C. Atesin, Oscar Rodriguez, Diego Rivera, Lohany Y. Garcia

Department of Chemistry, The University of Texas Rio Grande Valley, Edinburg, Texas 78539-2999, United States

E-mail address: tulay.atesin@utrgv.edu

Abstract

The most stable conformations of a TADDOL-based phosphoramidite *P*,*N* ligand coordinated to a palladium(II) η^3-π-allyl fragment have been investigated using molecular mechanical and quantum mechanical calculations. The conformational analysis initially generated 53 unique structures within 5 kcal/mol and subsequent geometry optimization narrowed the number of low-energy conformers down to 13. The two lowest energy conformers differ mainly in the conformation of the allyl group. The conformer with an endo allyl group has a slightly higher relative energy than the conformer with an exo allyl group. Comparison of the main geometric parameters around the Pd(II) metal center in the two lowest energy conformers with the available X-ray single crystal structures of Pd(II) η^3-π-allyl complexes of *P*,*N* ligands shows a good agreement in both the bond lengths and angles. The lowest energy structure has a "chair" conformation of the seven-membered phospha-dioxa-cycloheptane ring and "edge-on/face-on/face-on/edge-on" arrangement of the phenyl rings. The next lowest energy conformer with an exo allyl group has a "twist" conformation of the seven-membered ring and alternating "edge-on" and "face-on" arrangement of the phenyl rings as anticipated from the Knowles "edge-on/face-on" concept. The results of this study support published hypotheses regarding the origin of the chiral induction in the enantioselective Pd(0) catalyzed intramolecular allylic alkylation reaction by the repulsive interactions between one of the phenyl groups in the seven-membered ring in the lowest energy conformer of the ligand with the substrate. As such, the results of this research can be used to guide the synthesis of new and improved variants of this important catalyst family.

Keywords: TADDOL; Phosphoramidite; *P*,*N* ligands; Palladium(II); Conformational search; DFT

1. Introduction

TetraAryl-1,3-Dioxolane-4,5-DimethanOL(TADDOL)-based phosphoramidites (**Scheme 1**) are exceptionally versatile chiral ligands that have found a wide range of applications in asymmetric transition-metal catalysis [1–6]. The extraordinary attractiveness of this ligand class is due to their robustness, ease of synthesis in enantiomerically pure form from inexpensive tartrate esters and their modular structure that allows for a quick assembly of a ligand library. The ketal backbone, the aryl groups and the substituents on the amine group are the three areas for introducing diversity and can be varied independently to provide diverse ligands from easily accessible starting materials. The steric and electronic characteristics of the ligand can be fine-tuned by modifying the ketal, aryl and amine substituents.

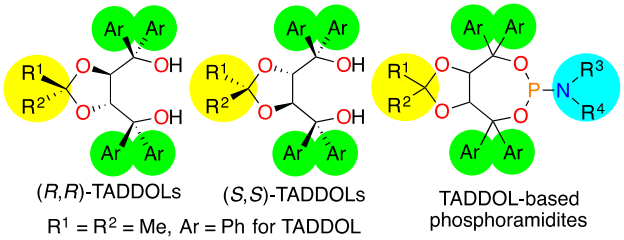

Scheme 1. Structure of α,α,α,α-tetraaryl-1,3-dioxolane-4,5-dimethanols (TADDOLs) and TADDOL-based phosphoramidites

TADDOL-based phosphoramidites enable high enantioselectivities in many impactful reactions, such as Nobel prize-winning class of palladium-catalyzed cross-coupling Heck [7–9]

and Suzuki [10–12] reactions; allylic alkylation [12–16], allylation [17–19], C–H functionalization [20–26] reactions and others [27–34]. Together with Tius, we reported the enantioselective Pd(0)-catalyzed "Nazarov-type" cyclization of diketoesters using a TADDOL-based phosphoramidite ligand incorporating a pyridine ring (**Scheme 2**) [35]. The nitrogen atom of the pyridyl substituent in the ligand provides a second weak coordination site and improves the asymmetry transfer by limiting the degrees of rotational freedom about the Pd-P axis in the metal-ligand complex [35–37]. Recently, using density functional theory (DFT) calculations, we demonstrated that this reaction is essentially a Pd(0)-catalyzed intramolecular asymmetric allylic alkylation [38]. Our proposed mechanism contains a Pd(0)-Pd(II)-Pd(0) catalytic cycle involving a key Pd(II) η^3-π-allyl intermediate that leads to the lowest energy pathway for the cyclization and explains the experimentally observed enantioselectivity of this reaction.

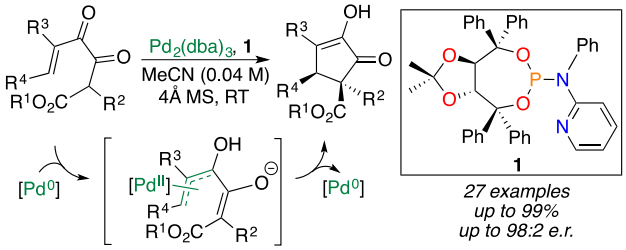

Scheme 2. Proposed Pd(II) η^3-π-allyl intermediate in the Pd(0)-catalyzed intramolecular asymmetric allylic alkylation

It is remarkable, given their widespread use and utility, that to date there is limited structural information available on the palladium(II) complexes of TADDOL-based phosphoramidite ligands [15]. In our previous studies [35], we based our computational model on the available X-ray single crystal structures of a monodentate TADDOL-based phosphoramidite ligand [39] and Pd(II) η^3-π-allyl complexes of *P*,*N* ligands [40,41] (**Scheme 3**). To address this deficiency, in this study, the conformational space of Pd(II) η^3-π-allyl complexes of TADDOL-based phosphoramidite *P*,*N* ligands, **2**, is explored using molecular mechanical (MM) and quantum mechanical (QM) methods. To the best of our knowledge, no conformational data have been reported on the Pd(II) η^3-π-allyl complexes of TADDOL-based phosphoramidite *P*,*N* ligands.

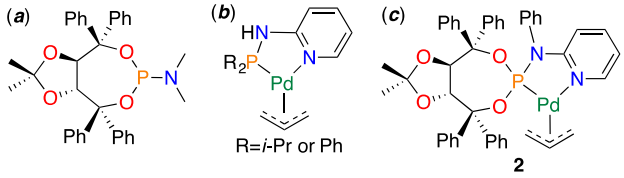

Scheme 3. (***a***) Monodentate TADDOL-based phosphoramidite ligand, (***b***) Pd(II) η^3-π-allyl complexes of *P*,*N* ligands in reference 40, and (***c***) proposed structure of a Pd(II) η^3-π-allyl complex of a TADDOL-based phosphoramidite *P*,*N* ligand.

2. Computational details

The search for low-energy conformers of **2** was performed by first generating all of the plausible conformers using MM methods followed by geometry optimization using QM methods.

2.1. MM Methods

Molecular mechanical calculations were performed using Schrödinger's Macromodel 11.8 [42]. Conformational searches were performed using the mixed Monte Carlo/Low Mode (MC/LMOD) methods [43] and the OPLS3 force field [44] as implemented in the Macromodel software. The dielectric constant (ε) was set at 36.64 for acetonitrile. Three independent conformational searches with a maximum number of 200,000 steps was conducted. A 100,000-step conformational search also gave similar results. All 53 non-hydrogen atoms were used for comparison when eliminating redundant conformers. The energy window for saving structures was set to 5 kcal/mol. The Truncated Newton Conjugate Gradient (TNCG) minimization method with an energy convergence threshold of 0.01 kcal/(mol Å) was used for the geometry optimization [45].

The structures with relative energies lower than 5 kcal/mol after 100,000 minimization iterations were further optimized by QM methods. The starting geometry of **2** was generated from the available X-ray single crystal structures of a monodentate TADDOL-based phosphoramidite ligand [39] and Pd(II) η^3-π-allyl complexes of *P*,*N* ligands [40] and optimized by DFT before the conformational search. The numbering of the atoms of **2** is displayed in **Fig. 1**. The torsional angles C(2)-Pd(1)-P(18)-N(11) and C(4)-Pd(1)-N(5)-C(10) were constrained to preserve the square-planar coordination environment around the Pd(II) metal center. The C(5) and C(8) atoms are fixed as chiral centers. All single bonds were allowed to rotate, except the bonds involved in the ring closures (N(11)-P(18), C(20)-C(33) and C(33)-O(34)) and constrained bonds (**Fig. 2**).

2.2. QM Methods

All quantum mechanical calculations were performed using Gaussian 09 suite of programs [46]. The starting geometry of **2** and low-energy conformers found by MM methods were fully optimized in redundant internal coordinates without any symmetry constraints [47] with DFT and a wave function incorporating the hybrid functional of Truhlar and Zhao, M06 [48]. The Pd and P atoms were represented with the effective core pseudopotentials of the Stuttgart group and the associated basis sets improved with a set of *f*-polarization functions for Pd (α=1.472) [49] and a set of *d*-polarization functions for P (α =0.387) [50]. The remaining atoms (C, H, N and O) were represented with the 6-31G(d,p) basis sets [51]. The geometries were fully optimized with tight convergence criteria and with ultrafine integration grid sizes. The effect of the solvent on the geometries and the relative stabilities of the conformers were evaluated by using the Solvation Model based on Density (SMD) [52] and acetonitrile as the solvent. Frequency calculations were performed on the optimized geometries at the same level of theory in order to confirm that the obtained geometries have zero imaginary frequencies and to obtain vibrational zero-point energy, thermal and entropic corrections. Single-point energy calculations on the optimized geometries were performed using the M06 density functional with the same basis set detailed above for Pd and P, and the polarized and diffuse 6-311++G(d,p) [53,54] basis set for all of the other atoms. The free energy corrections were calculated by adding thermal corrections calculated from the SMD(CH_3CN) M06/SDD(d,f)-6-31G(d,p) unscaled vibrational frequencies to the SMD(CH_3CN) M06/SDD(d,f)-6-311++G(d,p) electronic energies. As in our previous work [38], energies discussed throughout the text are the Gibbs free energies at 298.15 K and 1 atm obtained by using Truhlar's quasiharmonic approximation [55,56], where the real harmonic vibrational frequencies that are lower than 100 cm^{-1} are set to 100 cm^{-1} Optimized structures are illustrated using UCSF Chimera [57].

3. Results and discussion

*3.1. Conformational search and conformer optimization of **2***

The conformational search of **2** using MM methods ended with 53 unique structures stored, which were then optimized by QM methods. A comparison of the overlays of the wire representations of all of the 53 conformers of **2** from MM and QM calculations using M06 functional are shown in **Fig. 3** and their relative energies are tabulated in the supporting information (**Tables S1** and **S2)**. There are two sets of structures that differ in the relative conformation of the allyl group, conformers with the allyl group "down" (endo) and those with the allyl group "up" (exo). During the conformational search, the square-planar palladium(II) coordination environment is preserved due to the torsional restrictions imposed. There are minimal conformational changes in the relatively rigid *trans*-fused bicyclo[5.3.0]decane skeleton. The conformational space spanned by the ketal moiety, phenyl and pyridyl groups during the conformational search is preserved after geometry optimization. A careful analysis of the optimized structures by QM methods using M06 functional showed that the 53 unique conformers of **2** initially generated by MM methods converged to 13 distinct conformers (see SI **Fig. S1)**.

During the conformational search by MM methods, the dihedral angle C(39)-C(33)-O(34)-C(35) of the ketal moiety spanned a range of 33.3° and indicates the extent of ring puckering in the five-membered dioxolane ring (**Table 1**). Dihedral angles O(19)-C(20)-C(27)-C(28), C(33)-C(20)-C(21)-C(22), C(39)-C(40)-C(47)-C(48) and O(53)-C(40)-C(41)-C(42) changed over a range of 77.4°, 96.7°, 131.0° and 71.2°, respectively. The change in these angles indicate the free rotations of the phenyl rings on the seven-membered phospha-dioxa-cycloheptane ring. The conformations of the seven-membered ring will be discussed in detail in section 3.3. The extent of rotations of the phenyl group on N(11) and that of the pyridyl group are measured by the dihedral angles P(18)-N(11)-C(12)-C(17) and N(5)-C(10)-N(11)-P(18), respectively. The range of these angles, 114.1° and 65.5°, indicate that the phenyl group on N(11) is more flexible than the pyridyl group due to being coordinated to the Pd(II) metal center through N(5). After geometry optimization by QM methods, the conformational space spanned by these dihedral angles during the conformational search is preserved. A complete list of selected dihedral angles in all of the 53 structures are tabulated in the supporting information (**Tables S1** and **S2**).

3.2. The lowest energy conformers

After geometry optimization by QM methods using M06 functional, the resulting two lowest energy conformers **2.1** and **2.2** differ mainly in the conformation of the allyl group (**Fig. 4**). Conformer **2.1** is the global minimum with an exo allyl group. Conformer **2.2** has an endo allyl group and exhibits a slightly higher relative energy of 0.2 kcal/mol than **2.1**. There is a very good overlap with respect to the *trans*-fused bicyclo[5.3.0]decane skeleton and the phenyl groups on the phospha-dioxa-cycloheptane ring as can be seen from their overlay (**Fig. 5a**). They differ mainly in the relative conformations of the allyl group, the pyridyl group and the phenyl group on N(11), primarily due to the repulsive interactions between the allyl and the pyridyl groups (**Fig. 5b**). The conformers, where the allyl and the pyridyl groups are on the same side of the Pd(1)-P(18)-N(11) plane, have relatively higher energies due to these repulsive forces. Optimized structures of all of the conformers are collected in the supporting information (**Fig. S1**).

Comparison of the main geometric parameters around the Pd(II) metal center in **2.1** and **2.2** with the available X-ray single crystal structures of Pd(II) η^3-π-allyl complexes of *P*,*N* ligands [40] shows a good agreement in both the bond lengths and angles (Table **2**). In the solid-state structure of a Pd(II) η^3-π-allyl complex of a TADDOL-derived phosphoramidite ligand, an η^2-arene stabilization was observed by the coordination of the ligand to the Pd(II) metal center through its P atom and one of the aryl rings [15]. In the case of **2**, the coordination of the basic

pyridine N atom to the Pd(II) metal center blocks this type of interaction between the phenyl rings and the Pd(II) metal center.

3.3. Main structural differences between conformers

Twelve unique conformers initially generated by MM methods converged to structures that are very similar to **2.1** after geometry optimization by QM methods, with only minor differences in the pyridyl ring orientation. The N(5)-C(10)-N(11)-P(18) dihedral angle varies by 2.8° from -9.8° in **2.1** and the relative energies calculated by M06 functional change by 0.3 kcal/mol within this group. An overlay of these 12 optimized structures with **2.1** is shown in the supporting information together with overlays of all of the other related conformers (**Fig. S1**). Similarly, a cluster of 10 unique conformers converged to structures comparable to **2.2**. The variation in the N(5)-C(10)-N(11)-P(18) dihedral angle in this group is 1.5° from 8.1° in **2.2** and the relative energy range is 0.2 - 0.4 kcal/mol.

Among the 13 distinct conformers obtained after geometry optimization by QM methods, **2.1**, **2.3**, **2.6**, **2.8**, **2.9**, **2.12** and **2.13** have an exo allyl group and **2.2**, **2.4**, **2.5**, **2.7**, **2.10** and **2.11** have an endo allyl group (**Table 3**). The structure of **2.3** is similar to that of **2.1** with a N(5)-C(10)-N(11)-P(18) dihedral angle of 2.2° in **2.3** compared to -9.8° in **2.1**. Since the allyl group and the pyridyl ring are on the same side of the Pd(1)-P(18)-N(11) plane in **2.3**, its relative energy is 0.4 kcal/mol higher than that of **2.1**. Similarly, **2.4** has a N(5)-C(10)-N(11)-P(18) dihedral angle of -4.5° compared to 8.1° in **2.2** as the main difference. The relative energy of 0.4 kcal/mol with respect to **2.2** is due to the repulsion between the allyl group and the pyridyl ring on the same side of the Pd(1)-P(18)-N(11) plane. Due to the similarities between the complexes with exo and endo allyl groups, only the conformers with an exo allyl group will be discussed further.

The next lowest energy conformer with an exo allyl group is **2.6** with a relative free energy of 2.4 kcal/mol. The seven-membered phospha-dioxa-cycloheptane ring adopts a “twist” conformation in **2.6** in contrast to the “chair” conformation in **2.1** (**Fig. 6**). This conformation has been observed in TADDOL-based phosphoramidite ligands coordinated to Rh [58], Pt [59] and Au [60] metal centers. Similar to TADDOLs [2], both **2.1** and **2.6** display an antiperiplanar arrangement of dioxolane and phospha-dioxa-cycloheptane C-O bonds, along with quasi-axial (q-a) and quasi-equatorial(q-e) placement of the geminal phenyl groups. An “edge-on” conformation is preferred for the q-a position and “face-on” conformation for the q-e position. The alternating “edge-on” and “face-on” arrangement of the phenyl rings in **2.6** aligns with the Knowles “edge-on/face-on” concept (**Fig. 7**)[61–63]. Due to the free rotations of the phenyl rings, it was proposed that the “edge-on/face-on” concept is not important in TADDOL as much as it is in tetra(1-naphthyl) TADDOLs [61]. The deviation from this concept in the lowest energy conformer **2.1**, that has “edge-on/face-on/face-on/edge-on” arrangement of the phenyl rings, is consistent with this proposal.

4. Conclusions

The conformational analysis of a TADDOL-based phosphoramidite *P*,*N* ligand coordinated to a Pd(II) η^3-π-allyl fragment initially generated 53 unique structures using MM methods. Two lowest energy conformers, after the subsequent geometry optimization with QM methods, differ mainly in the conformation of the allyl group. The conformer with an exo allyl group is the global minimum. Comparison of the main geometric parameters around the Pd(II) metal center with the available X-ray single crystal structures of Pd(II) η^3-π-allyl complexes of *P*,*N* ligands shows a

good agreement in the bond lengths and angles. The lowest energy structure has a “chair” conformation of the phospha-dioxa-cycloheptane ring and “edge-on/face-on/face-on/edge-on” arrangement of the phenyl rings, which is different than a propeller-like arrangement of the phenyl rings commonly reported in the X-ray single crystal structures of TADDOL. We previously based the origin of the chiral induction in the enantioselective Pd(0) catalyzed intramolecular allylic alkylation reactions on the repulsive interactions between this conformer of the ligand and the substrate [35]. The results of this study support our earlier proposal. The next lowest energy conformer with an exo allyl group has an alternating “edge-on” and “face-on” arrangement of the phenyl rings as anticipated from the Knowles “edge-on/face-on” concept and a “twist” conformation of the phospha-dioxa-cycloheptane ring. The 2.4 kcal/mol energy difference between the “chair” and “twist” conformations of the phospha-dioxa-cycloheptane ring can easily be overcome by the steric interactions between the phenyl groups on the seven-membered ring and substituents on the allyl group. Therefore, it is important to consider possible changes in the ligand conformation with different substrates to explain the stereochemical outcome of the reaction, and to design new catalysts. The conclusions drawn from this study is valuable for understanding the chiral induction in enantioselective palladium catalyzed allylic alkylation reactions enabled by TADDOL-based phosphoramidite *P*,*N* ligands.

Acknowledgments

T.A.A. gratefully acknowledges Dr. Thomas R. Cundari and Dr. Kristine L. Lowe for valuable criticism, the Texas Advanced Computing Center (TACC) at The University of Texas at Austin for providing HPC resources that have contributed to the research results reported within this paper (URL: http://www.tacc.utexas.edu) and support through The University of Texas Rio Grande Valley (UTRGV) ADVANCE Program funded by the National Science Foundation (Award # 1209210), UTRGV Science Education Grant Program #52007568 funded by the Howard Hughes Medical Institute (HHMI) and UTRGV College of Sciences Research Enhancement Seed Grants Program. The Department of Chemistry at UTRGV is grateful for the generous support provided by a Departmental Grant from the Robert A. Welch Foundation (Grant No. BX-0048).

Appendix A. Supplementary material

Supplementary data associated with this article can be found, in the online version, at …

References

[1] B.L. Feringa, Phosphoramidites: Marvellous ligands in catalytic asymmetric conjugate addition, Acc. Chem. Res. 33 (2000) 346–353. doi:10.1021/ar990084k.

[2] D. Seebach, A.K. Beck, A. Heckel, TADDOLs, their derivatives, and TADDOL analogues: Versatile chiral auxiliaries, Angew. Chemie - Int. Ed. 40 (2001) 92–138. doi:10.1002/1521-3773(20010105)40.

[3] H. Pellissier, Use of TADDOLs and their derivatives in asymmetric synthesis, Tetrahedron. 64 (2008) 10279–10317. doi:10.1016/j.tet.2008.08.029.

[4] J.F. Teichert, B.L. Feringa, Phosphoramidites: Privileged ligands in asymmetric catalysis, Angew. Chemie - Int. Ed. 49 (2010) 2486–2528. doi:10.1002/anie.200904948.

[5] H.W. Lam, TADDOL-derived phosphonites, phosphites, and phosphoramidites in asymmetric catalysis, Synthesis (Stuttg). (2011) 2011–2043. doi:10.1055/s-0030-1260022.

[6] J. Pedroni, N. Cramer, TADDOL-based phosphorus(III)-ligands in enantioselective Pd(0)-catalysed C–H functionalisations, Chem. Commun. 51 (2015) 17647–17657. doi:10.1039/C5CC07929B.

[7] R. Imbos, A.J. Minnaard, B.L. Feringa, A highly enantioselective intramolecular heck reaction with a monodentate ligand, J. Am. Chem. Soc. 124 (2002) 184–185. doi:10.1021/ja017200a.

[8] R. Imbos, A.J. Minnaard, B.L. Feringa, Monodentate phosphoramidites; versatile ligands in catalytic asymmetric intramolecular Heck reactions, Dalt. Trans. (2003) 2017–2023. doi:10.1039/B300565H.

[9] S. Mannathan, S. Raoufmoghaddam, J.N.H. Reek, J.G. de Vries, A.J. Minnaard, Enantioselective Intramolecular Reductive Heck Reaction with a Palladium/Monodentate Phosphoramidite Catalyst, ChemCatChem. 9 (2017) 551–554. doi:10.1002/cctc.201601153.

[10] A. Ros, B. Estepa, P. Ramírez-López, E. Álvarez, R. Fernández, J.M. Lassaletta, Dynamic kinetic cross-coupling strategy for the asymmetric synthesis of axially chiral heterobiaryls, J. Am. Chem. Soc. 135 (2013) 15730–15733. doi:10.1021/ja4087819.

[11] H.-Y. Sun, D.G. Hall, K. Kubota, Reaction Optimization, Scalability, and Mechanistic Insight on the Catalytic Enantioselective Desymmetrization of 1,1-Diborylalkanes via Suzuki-Miyaura Cross-Coupling, Chemistry. 21 (2015) 19186–19194.

[12] R.P.J. Bronger, P.J. Guiry, Aminophosphine-oxazoline and phosphoramidite-oxazoline ligands and their application in asymmetric catalysis, Tetrahedron Asymmetry. 18 (2007) 1094–1102.

[13] Z.D. Jiang, Z.H. Meng, Polymer-supported chiral monodentate phosphoramidites in palladium-catalyzed allylic alkylation reactions, Chinese J. Chem. 25 (2007) 542–545. doi:10.1002/cjoc.200790101.

[14] M.D.K. Boele, P.C.J. Kamer, M. Lutz, A.L. Spek, J.G. de Vries, P.W.N.M. Van Leeuwen, G.P.F. Van Strijdonck, Bulky monodentate phosphoramidites in palladium-catalyzed allylic alkylation reactions: Aspects of regioselectivity and enantioselectivity, Chem. - A Eur. J. 10 (2004) 6232–6246. doi:10.1002/chem.200400154.

[15] B.-S. Zeng, X. Yu, P.W. Siu, K.A. Scheidt, Catalytic enantioselective synthesis of 2-aryl-chromenes, Chem. Sci. 5 (2014) 2277. doi:10.1039/c4sc00423j.

[16] K.N. Gavrilov, S. V. Zheglov, I. V. Chuchelkin, M.G. Maksimova, I.D. Firsin, A.N. Fitch, V. V. Chernyshev, A. V. Maximychev, A.M. Perepukhov, Tartaric acid-derived chiral phosphite-type P,N-ligands: behavioural features in Pd-catalyzed asymmetric transformations, Tetrahedron Asymmetry. 28 (2017) 1633–1643. doi:10.1016/j.tetasy.2017.09.011.

[17] L.A. Brozek, J.D. Sieber, J.P. Morken, Catalytic enantioselective conjugate allylation of unsaturated methylidene ketones, Org. Lett. 13 (2011) 995–997. doi:10.1021/ol102982b.

[18] K.N. Gavrilov, S. V. Zheglov, I.M. Novikov, I. V. Chuchelkin, V.K. Gavrilov, V. V. Lugovsky, I.A. Zamilatskov, Palladium-catalyzed enantioselective allylation in the presence of phosphoramidites derived from (Sa)-3-SiMe3-BINOL, (R,S)-semi-TADDOL, and (R,R)-TADDOL, Russ. Chem. Bull. 64 (2015) 1595–1601. doi:10.1007/s11172-015-1047-7.
[19] Y.L. Su, Z.Y. Han, Y.H. Li, L.Z. Gong, Asymmetric Allylation of Furfural Derivatives: Synergistic Effect of Chiral Ligand and Organocatalyst on Stereochemical Control, ACS Catal. 7 (2017) 7917–7922. doi:10.1021/acscatal.7b02667.
[20] M.R. Albicker, N. Cramer, Enantioselective palladium-catalyzed direct arylations at ambient temperature: access to indanes with quaternary stereocenters, Angew. Chemie - Int. Ed. 48 (2009) 9139–9142. doi:10.1002/anie.200905060.
[21] T. Saget, N. Cramer, Enantioselective C-H arylation strategy for functionalized dibenzazepinones with quaternary stereocenters, Angew. Chemie - Int. Ed. 52 (2013) 7865–7868. doi:10.1002/anie.201303816.
[22] L. Liu, A.A. Zhang, R.J. Zhao, F. Li, T.J. Meng, N. Ishida, M. Murakami, W.X. Zhao, Asymmetric synthesis of planar chiral ferrocenes by enantioselective intramolecular C-H arylation of N-(2-haloaryl)ferrocenecarboxamides, Org. Lett. 16 (2014) 5336–5338. doi:10.1021/ol502520b.
[23] J. Pedroni, M. Boghi, T. Saget, N. Cramer, Access to β-lactams by enantioselective palladium(0)-catalyzed C(sp3)-H alkylation, Angew. Chemie - Int. Ed. 53 (2014) 9064–9067. doi:10.1002/anie.201405508.
[24] J. Pedroni, T. Saget, P.A. Donets, N. Cramer, Enantioselective palladium(0)-catalyzed intramolecular cyclopropane functionalization: access to dihydroquinolones, dihydroisoquinolones and the BMS-791325 ring system, Chem. Sci. 6 (2015) 5164–5171. doi:10.1039/C5SC01909E.
[25] L. Liu, A.A. Zhang, Y. Wang, F. Zhang, Z. Zuo, W.X. Zhao, C.L. Feng, W. Ma, Asymmetric Synthesis of P-Stereogenic Phosphinic Amides via Pd(0)-Catalyzed Enantioselective Intramolecular C-H Arylation, Org. Lett. 17 (2015) 2046–2049. doi:10.1021/acs.orglett.5b00122.
[26] Z.Q. Lin, W.Z. Wang, S.B. Yan, W.L. Duan, Palladium-catalyzed enantioselective C-H arylation for the synthesis of P-stereogenic compounds, Angew. Chemie - Int. Ed. 54 (2015) 6265–6269. doi:10.1002/anie.201500201.
[27] N.F. Pelz, A.R. Woodward, H.E. Burks, J.D. Sieber, J.P. Morken, Palladium-catalyzed enantioselective diboration of prochiral allenes, J. Am. Chem. Soc. 126 (2004) 16328–16329. doi:10.1021/ja044167u.
[28] A.R. Woodward, H.E. Burks, L.M. Chan, J.P. Morken, Concatenated catalytic asymmetric allene diboration/allylation/ functionalization, Org. Lett. 7 (2005) 5505–5507. doi:10.1021/ol052312i.
[29] T. Ohmura, H. Taniguchi, M. Suginome, Palladium-catalyzed asymmetric silaboration of allenes, J. Am. Chem. Soc. 128 (2006) 13682–13683. doi:10.1021/ja063934h.
[30] H.E. Burks, S. Liu, J.P. Morken, Development, mechanism, and scope of the palladium-catalyzed enantioselective allene diboration, J. Am. Chem. Soc. 129 (2007) 8766–8773. doi:10.1021/ja070572k.
[31] Y. Kurihara, M. Nishikawa, Y. Yamanoi, H. Nishihara, Synthesis of optically active tertiary silanes via Pd-catalyzed enantioselective arylation of secondary silanes, Chem. Commun. 48 (2012) 11564. doi:10.1039/c2cc36238d.
[32] C.H. Schuster, J.R. Coombs, Z.A. Kasun, J.P. Morken, Enantioselective carbocycle formation through intramolecular Pd-catalyzed allyl-aryl cross-coupling, Org. Lett. 16 (2014) 4420–4423. doi:10.1021/ol5019163.
[33] J. Feng, B. Li, Y. He, Z. Gu, Enantioselective synthesis of atropisomeric vinyl arene compounds by palladium catalysis: A carbene strategy, Angew. Chemie - Int. Ed. 55

(2016) 2186–2190. doi:10.1002/anie.201509571.
[34] L. Chen, J.-B. Huang, Z. Xu, Z.-J. Zheng, K.-F. Yang, Y.-M. Cui, J. Cao, L.-W. Xu, Palladium-catalyzed Si-C bond-forming silylation of aryl iodides with hydrosilanes: an enhanced enantioselective synthesis of silicon-stereogenic silanes by desymmetrization., RSC Adv. 6 (2016) 67113–67117. doi:10.1039/C6RA12873D.
[35] K. Kitamura, N. Shimada, C. Stewart, A.C. Atesin, T.A. Ateşin, M.A. Tius, Enantioselective palladium(0)-catalyzed nazarov-type cyclization, Angew. Chemie - Int. Ed. 54 (2015) 6288–6291. doi:10.1002/anie.201500881.
[36] Z. Zhou, M.A. Tius, Synthesis of each enantiomer of rocaglamide by means of a palladium(0)-catalyzed nazarov-type cyclization, Angew. Chemie - Int. Ed. 54 (2015) 6037–6040. doi:10.1002/anie.201501374.
[37] Z. Zhou, D.D. Dixon, A. Jolit, M.A. Tius, The Evolution of the Total Synthesis of Rocaglamide, Chem. - A Eur. J. 22 (2016) 15929–15936. doi:10.1002/chem.201603312.
[38] T.A. Ateşin, G.M. Martinez, D. Flores, It Is Not Just Up to the Substrate: Palladium(0) Cyclizes Nazarov Substrates through Intramolecular Allylic Alkylation, Organometallics. 36 (2017) 3589–3596. doi:10.1021/acs.organomet.7b00494.
[39] E. Keller, J. Maurer, R. Naasz, T. Schader, A. Meetsma, B.L. Feringa, Unexpected enhancement of enantioselectivity in copper(II) catalyzed conjugate addition of diethylzinc to cyclic enones with novel TADDOL phosphorus amidite ligands, Tetrahedron Asymmetry. 9 (1998) 2409–2413. doi:10.1016/S0957-4166(98)00240-7.
[40] D. Benito-Garagorri, K. Mereiter, K. Kirchner, Synthesis and characterization of Ni(II) and Pd(II) complexes bearing achiral and chiral bidentate aminophosphine ligands., Collect. Czechoslov. Chem. Commun. 72 (2007) 527–540. doi:10.1135/cccc20070527.
[41] B. Bichler, L.F. Veiros, Ö. Öztopcu, M. Puchberger, K. Mereiter, K. Matsubara, K.A. Kirchner, Synthesis, Structure, Ligand Dynamics, and Catalytic Activity of Cationic [Pd(η3-allyl)(κ2(E,N)-EN-chelate)]+ (E = P, O, S, Se) Complexes, Organometallics. 30 (2011) 5928–5942. doi:10.1021/om200766y.
[42] MacroModel, Version 11.8., Schrödinger, LLC, New York, NY, (2018).
[43] I. Kolossváry, W.C. Guida, Low-mode conformational search elucidated: Application to C39H80 and flexible docking of 9-deazaguanine inhibitors into PNP, J. Comput. Chem. 20 (1999) 1671–1684. doi:10.1002/(SICI)1096-987X(19991130)20:15<1671::AID-JCC7>3.0.CO;2-Y.
[44] E. Harder, W. Damm, J. Maple, C. Wu, M. Reboul, J.Y. Xiang, L. Wang, D. Lupyan, M.K. Dahlgren, J.L. Knight, J.W. Kaus, D.S. Cerutti, G. Krilov, W.L. Jorgensen, R. Abel, R.A. Friesner, OPLS3: A Force Field Providing Broad Coverage of Drug-like Small Molecules and Proteins, J. Chem. Theory Comput. 12 (2016) 281–296. doi:10.1021/acs.jctc.5b00864.
[45] J.W. Ponder, F.M. Richards, An efficient newton-like method for molecular mechanics energy minimization of large molecules, J. Comput. Chem. 8 (1987) 1016–1024. doi:10.1002/jcc.540080710.
[46] M.J. Frisch, G.W. Trucks, H.B. Schlegel, G.E. Scuseria, M.A. Robb, J.R. Cheeseman, G. Scalmani, V. Barone, B. Mennucci, G.A. Petersson, H. Nakatsuji, M. Caricato, X. Li, H.P. Hratchian, A.F. Izmaylov, J. Bloino, G. Zheng, J.L. Sonnenberg, M. Hada, M. Ehara, K. Toyota, R. Fukuda, J. Hasegawa, M. Ishida, T. Nakajima, Y. Honda, O. Kitao, H. Nakai, T. Vreven, J. Montgomery, J. A., J.E. Peralta, F. Ogliaro, M. Bearpark, J.J. Heyd, E. Brothers, K.N. Kudin, V.N. Staroverov, R. Kobayashi, J. Normand, K. Raghavachari, A. Rendell, J.C. Burant, S.S. Iyengar, J. Tomasi, M. Cossi, N. Rega, N.J. Millam, M. Klene, J.E. Knox, J.B. Cross, V. Bakken, C. Adamo, J. Jaramillo, R. Gomperts, R.E. Stratmann, O. Yazyev, A.J. Austin, R. Cammi, C. Pomelli, J.W. Ochterski, R.L. Martin, K. Morokuma, V.G. Zakrzewski, G.A. Voth, P. Salvador, J.J. Dannenberg, S. Dapprich, A.D. Daniels, Ö. Farkas, J.B. Foresman, J. V. Ortiz, J. Cioslowski, D.J. Fox, Gaussian 09, Revision D.01,

Gaussian Inc., Wallingford. (2013). doi:10.1017/CBO9781107415324.004.
[47] C. Peng, P.Y. Ayala, H.B. Schlegel, M.J. Frisch, Using redundant internal coordinates to optimize equilibrium geometries and transition states, J. Comput. Chem. 17 (1996) 49–56. doi:10.1002/(SICI)1096-987X(19960115)17:1<49::AID-JCC5>3.0.CO;2-0.
[48] Y. Zhao, D.G. Truhlar, The M06 suite of density functionals for main group thermochemistry, thermochemical kinetics, noncovalent interactions, excited states, and transition elements: Two new functionals and systematic testing of four M06-class functionals and 12 other function, Theor. Chem. Acc. 120 (2008) 215–241. doi:10.1007/s00214-007-0310-x.
[49] A.W. Ehlers, M. Böhme, S. Dapprich, A. Gobbi, A. Höllwarth, V. Jonas, K.F. Köhler, R. Stegmann, A. Veldkamp, G. Frenking, A set of f-polarization functions for pseudo-potential basis sets of the transition metals ScCu, YAg and LaAu, Chem. Phys. Lett. 208 (1993) 111–114. doi:10.1016/0009-2614(93)80086-5.
[50] A. Höllwarth, M. Böhme, S. Dapprich, A.W. Ehlers, A. Gobbi, V. Jonas, K.F. Köhler, R. Stegmann, A. Veldkamp, G. Frenking, A set of d-polarization functions for pseudo-potential basis sets of the main group elements AlBi and f-type polarization functions for Zn, Cd, Hg, Chem. Phys. Lett. 208 (1993) 237–240. doi:10.1016/0009-2614(93)89068-S.
[51] W.J. Hehre, R. Ditchfield, J.A. Pople, Self—Consistent Molecular Orbital Methods. XII. Further Extensions of Gaussian—Type Basis Sets for Use in Molecular Orbital Studies of Organic Molecules, J. Chem. Phys. 56 (1972) 2257–2261. doi:10.1063/1.1677527.
[52] A. V. Marenich, C.J. Cramer, D.G. Truhlar, Universal solvation model based on solute electron density and on a continuum model of the solvent defined by the bulk dielectric constant and atomic surface tensions, J. Phys. Chem. B. 113 (2009) 6378–6396. doi:10.1021/jp810292n.
[53] A.D. McLean, G.S. Chandler, Contracted Gaussian basis sets for molecular calculations. I. Second row atoms, Z=11-18, J. Chem. Phys. 72 (1980) 5639–5648. doi:10.1063/1.438980.
[54] R. Krishnan, J.S. Binkley, R. Seeger, J.A. Pople, Self-consistent molecular orbital methods. XX. A basis set for correlated wave functions, J. Chem. Phys. 72 (1980) 650–654. doi:10.1063/1.438955.
[55] R.F. Ribeiro, A. V. Marenich, C.J. Cramer, D.G. Truhlar, Use of solution-phase vibrational frequencies in continuum models for the free energy of solvation, J. Phys. Chem. B. 115 (2011) 14556–14562. doi:10.1021/jp205508z.
[56] Y. Zhao, D.G. Truhlar, Computational characterization and modeling of buckyball tweezers: density functional study of concave–convex π···π interactions, Phys. Chem. Chem. Phys. 10 (2008) 2813. doi:10.1039/b717744e.
[57] E.F. Pettersen, T.D. Goddard, C.C. Huang, G.S. Couch, D.M. Greenblatt, E.C. Meng, T.E. Ferrin, UCSF Chimera—A Visualization System for Exploratory Research and Analysis, J Comput Chem. 25 (2004) 1605–1612. doi:10.1002/jcc.20084.
[58] D.M. Dalton, K.M. Oberg, R.T. Yu, E.E. Lee, S. Perreault, M.E. Oinen, M.L. Pease, G. Malik, T. Rovis, Enantioselective rhodium-catalyzed [2 + 2 + 2] cycloadditions of terminal alkynes and alkenyl isocyanates: Mechanistic insights lead to a unified model that rationalizes product selectivity, J. Am. Chem. Soc. 131 (2009) 15717–15728. doi:10.1021/ja905065j.
[59] Y. Zhang, H. Jullien, D. Brissy, P. Retailleau, A. Voituriez, A. Marinetti, Platinum(II) catalyzed enantioselective cycloisomerizations of 3-hydroxylated 1,5-enynes, ChemCatChem. 5 (2013) 2051–2057. doi:10.1002/cctc.201200743.
[60] H. Teller, S. Flügge, R. Goddard, A. Fürstner, Enantioselective gold catalysis: Opportunities provided by monodentate phosphoramidite ligands with an acyclic TADDOL backbone, Angew. Chemie - Int. Ed. 49 (2010) 1949–1953. doi:10.1002/anie.200906550.

[61] A.K. Beck, M. Dobler, D.A. Plattner, TADDOLs under Closer Scrutiny - Why Bulky Substituents Make It All Different, Helv. Chim. Acta. 80 (1997) 2073–2083. doi:10.1002/hlca.19970800708.
[62] I.Y. N., A. Xavier, B.A. K., B. Andrej, G. Camille, G.R. E., K.F.N. M., T. Juraj, W.Y. Ming, S. Dieter, Preparation and Structural Analysis of Several New α,α,α′,α′-Tetraaryl-1,3-dioxolane-4,5-dimethanols (TADDOL's) and TADDOL analogs, their evaluation as titanium ligands in the enantioselective addition of methyltitanium and diethylzinc reagents to benzald, Helv. Chim. Acta. 77 (2018) 2071–2110. doi:10.1002/hlca.19940770802.
[63] B.D. Vineyard, W.S. Knowles, M.J. Sabacky, G.L. Bachman, D.J. Weinkauff, Asymmetric Hydrogenation. Rhodium Chiral Bisphosphine Catalyst, J. Am. Chem. Soc. 99 (1977) 5946–5952. doi:10.1021/ja00460a018.

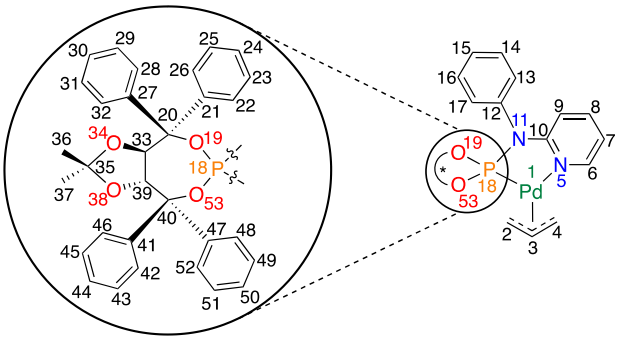

Fig. 1. Numbering of atoms in **2**.

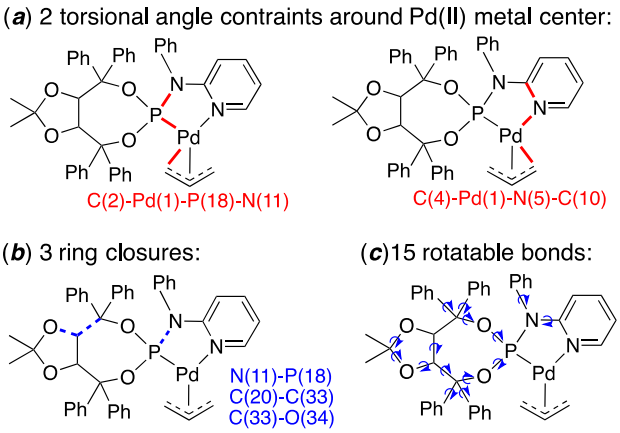

Fig. 2. Conformational search protocol for **2**. (***a***) The torsional angle constraints are shown in red, (***b***) the ring closures are shown with a dotted blue line, and (***c***) rotatable bonds are shown with blue arrows.

(***a***) top view

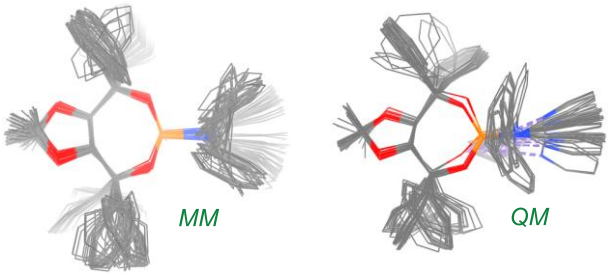

(***b***) bottom view

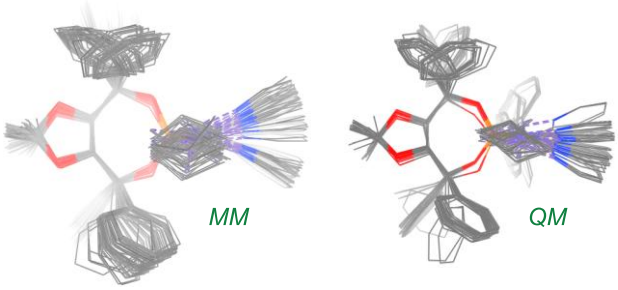

Fig. 3. A comparison of the overlays of the wire representations of all of the 53 conformers of **2** derived from the conformational search using MM methods and after geometry optimization by QM methods using M06 functional. (***a***) top view and (***b***) bottom view. Hydrogen atoms are omitted for clarity, gray: carbon; red: oxygen; orange: phosphorus; blue: nitrogen; ocean green: palladium (similarly hereinafter).

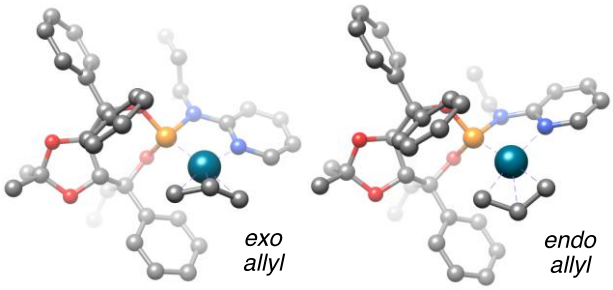

Fig. 4. Optimized geometries of the two lowest energy conformers of **2** and their relative free energies (ΔG) in kcal/mol calculated by M06 functional.

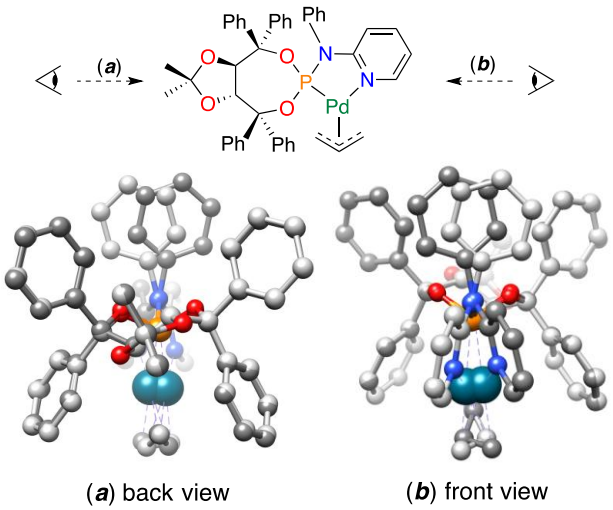

Fig. 5. (***a***) Back view and (***b***) front view of the overlay of **2.1** (shown in dark gray) and **2.2** (shown in light gray).

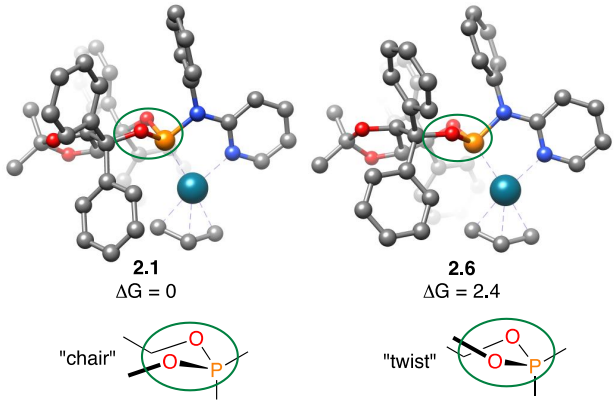

Fig. 6. "Chair" and "twist" conformations of the seven-membered phospha-dioxa-cycloheptane ring in the optimized geometries of the two lowest energy conformers with an exo ally group and their relative free energies (ΔG) in kcal/mol calculated by M06 functional.

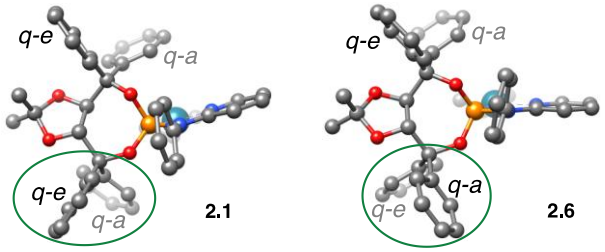

Fig. 7. Quasi-axial (q-a) and quasi-equatorial(q-e) placement of the phenyl groups.

Table 1. The minimum (min), maximum (max), average (ave) and standard deviation (SD) of selected dihedral angles (°) in the conformers of **2** derived from the conformational search by MM methods and after geometry optimization by QM methods using M06 functional.

	Conformational Search by MM				**Geometry Optimization by QM**			
Dihedral angles, θ	θ_{min} (°)	θ_{max} (°)	θ_{ave} (°)	**SD** (°)	θ_{min} (°)	θ_{max} (°)	θ_{ave} (°)	**SD** (°)
C(39)-C(33)-O(34)-C(35)	-37.6	-4.2	-22.4	12.0	-30.9	-1.8	-4.9	5.9
O(19)-C(20)-C(27)-C(28)	-60.0	17.4	-34.7	14.6	-42.7	56.2	-32.2	17.4
C(33)-C(20)-C(21)-C(22)	0.5	97.2	84.2	24.0	6.1	118.6	93.0	13.0
C(39)-C(40)-C(47)-C(48)	-101.3	29.7	-39.9	40.0	-77.0	12.8	-41.2	36.9
O(53)-C(40)-C(41)-C(42)	-22.9	48.3	12.9	29.2	-22.3	38.8	16.8	24.2
P(18)-N(11)-C(12)-C(17)	34.6	148.7	88.5	39.9	77.5	115.7	90.9	11.3
N(5)-C(10)-N(11)-P(18)	-36.0	29.6	2.2	24.7	-16.6	10.8	-1.6	8.2

Table 2. Comparison of the selected bond lengths (Å) and angles (°) around the Pd(II) metal center in conformers **2.1** and **2.2** with the Pd(II) complexes in reference 40, calculated using M06 functional. The numbers in parentheses are the experimental values measured from the X-ray single crystal structures.

	2.1	**2.2**	**MICXUS**[a]	**MICYAZ**[b]
Distances (Å)				
Pd(1)-C(2)	2.14	2.15	2.13 (*2.11*)	2.12 (*2.11*)
Pd(1)-C(3)	2.19	2.19	2.18 (*2.16*)	2.18 (*2.17*)
Pd(1)-C(4)	2.19	2.19	2.21 (*2.20*)	2.22 (*2.22*)
Pd(1)-N(5)	2.16	2.16	2.15 (*2.09*)	2.15 (*2.11*)
Pd(1)-P(18)	2.32	2.32	2.32 (*2.25*)	2.32 (*2.26*)
Angles (°)				
C(2)-Pd(1)-N(5)	171.1	171.1	172.9 (*173.3*)	173.7 (*174.1*)
C(4)-Pd(1)-P(18)	175.2	176.1	173.0 (*170.9*)	170.3 (*168.7*)

[a] MICXUS = $[C_{20}H_{20}N_2PPd]^+$; X-ray single crystal structure with R = Ph in **Scheme 3b**
[b] MICYAZ = $[C_{14}H_{24}N_2PPd]^+$; X-ray single crystal structure with R = *i*Pr in **Scheme 3b**.

Table 3. Low energy conformers of **2** and their relative free energies (ΔG) in kcal/mol calculated by M06 functional.

Structure	**ΔG (kcal/mol)**	**Structure**	**ΔG (kcal/mol)**
2.1	0.0	**2.8**	2.7
2.2	0.2	**2.9**	2.7
2.3	0.4	**2.10**	3.7
2.4	0.6	**2.11**	4.2
2.5	2.2	**2.12**	7.7
2.6	2.4	**2.13**	9.2
2.7	2.4		

GA

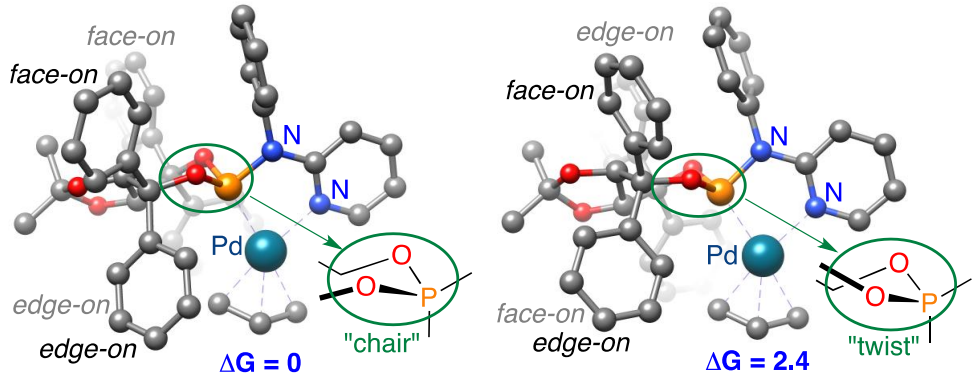
face-on
face-on
N
N
Pd
O
O
P
edge-on
edge-on
"chair"
ΔG = 0
edge-on
face-on
N
N
Pd
face-on
edge-on
O
O
P
"twist"
ΔG = 2.4

Highlights

Two lowest energy conformers differ in allyl conformation, conformer with exo allyl having lower energy

Lowest energy conformer has “chair” conformation of 7-membered ring and “edge-on/face-on/face-on/edge-on” array of Ph groups

Next lowest energy conformer with exo allyl has alternating “edge-on/face-on” arrangement and “twist” 7-membered ring

Changes in “chair/twist” conformations with different substrates is possible due to 2.4 kcal/mol energy difference

These results explain stereochemical outcome of the reaction, and will guide design of new catalysts